ENERGY RESOURCES

10.1126/sciadv.1500372

Three-dimensional graphene/Pt nanoparticle composites as freestanding anode for enhancing performance of microbial fuel cells

Shenlong Zhao,[1,2,3]* Yuchen Li,[1]* Huajie Yin,[3] Zhouzhou Liu,[1] Enxiao Luan,[1] Feng Zhao,[4] Zhiyong Tang,[3†] Shaoqin Liu[1†]

Microbial fuel cells (MFCs) are able to directly convert about 50 to 90% of energy from oxidation of organic matters in waste to electricity and have great potential application in broad fields such as wastewater treatment. Unfortunately, the power density of the MFCs at present is significantly lower than the theoretical value because of technical limitations including low bacteria loading capacity and difficult electron transfer between the bacteria and the electrode. We reported a three-dimensional (3D) graphene aerogel (GA) decorated with platinum nanoparticles (Pt NPs) as an efficient freestanding anode for MFCs. The 3D GA/Pt–based anode has a continuous 3D macroporous structure that is favorable for microorganism immobilization and efficient electrolyte transport. Moreover, GA scaffold is homogenously decorated with Pt NPs to further enhance extracellular charge transfer between the bacteria and the anode. The MFCs constructed with 3D GA/Pt–based anode generate a remarkable maximum power density of 1460 mW/m^2, 5.3 times higher than that based on carbon cloth (273 mW/m^2). It deserves to be stressed that 1460 mW/m^2 obtained from the GA/Pt anode shows the superior performance among all the reported MFCs inoculated with *Shewanella oneidensis* MR-1. Moreover, as a demonstration of the real application, the MFC equipped with the freestanding GA/Pt anode has been successfully applied in driving timer for the first time, which opens the avenue toward the real application of the MFCs.

INTRODUCTION

Treatment of organic wastewater currently needs both scientific and technical innovation because of huge energy costs; for instance, it consumes about 3 to 5% of all electrical power produced in the United States (*1*). Noteworthily, organic wastewater itself contains about nine times more energy than is needed for wastewater treatment (*2*). Thus, finding effective methods to use the energy stored in organic wastewater would not only decrease the energy consumption during wastewater treatment process but also offer novel routes to harvest the energy (*3*–*5*). Among different strategies, microbial fuel cells (MFCs), which directly convert the chemical energy of organic matter such as carbohydrate and organic acids to electricity using microorganisms, have received specific attention because of their dual benefit: using wastewater or complex solid waste as fuel to produce electrical power as well as reducing the biochemical oxygen demand loading of the wastewater with lower greenhouse emissions (*6*–*9*). Furthermore, in terms of energy balance, MFCs are able to directly convert about 50 to 90% of energy from oxidation of organic matters to electricity (*10*, *11*), so in theory the amount of power recovered from wastewater by MFCs can halve the electricity needed in whole wastewater treatment system (*12*). Actually, MFCs have demonstrated broad application prospects in wastewater treatment (*13*, *14*), bioremediation (*15*), toxic metal recovery (*16*), marine sediment (*17*), desalination (*18*–*20*), and energy recovery from human excrement in space (*21*). Unfortunately, the power density of the MFCs at present is significantly lower than the theoretical value (*22*–*25*). The observed low power should originate from current technical limitations such as low bacteria loading capacity and the difficult electron transfer between the bacteria and the electrode.

Among all the factors that affect the performance of MFCs, the selection and construction of anode materials are critical, which govern overall performance of MFCs (*26*–*29*). First, an ideal anode of MFCs that provides the accommodation space of bacteria requires porous structure and good biocompatibility, ensuring effective immobilization, growth and cultivation of living microorganisms, facile substrate transport to attached microorganisms, and easy removal of waste products. Second, the anode should be an excellent conductor to facilitate the electron transfer released from the microorganisms and efficient collection of currents from all regions of the electrode (*30*–*32*). Finally, for the real application of MFCs, an optimal anode needs high chemical and physical stabilities. A number of materials have been examined as the MFC anodes including noble metals (*23*–*25*), carbonaceous electrodes of distinct packing modes (for example, carbon cloth, graphite fiber brushes, carbon felt, carbon mesh, and carbon paper) (*33*–*39*), and conductive polymers and their composites (*40*–*44*). Although these anode materials bring considerable increment in the electric current, they are also reported to have some inherent drawbacks. For example, high cost and weak adhesion of inoculated bacteria prevent practical use of noble metal electrodes in MFCs. Although many features of the carbonaceous electrodes including the high mechanical strength, enhanced conductivity, eco-friendly composition, and cheap cost satisfy most of the requirements of MFC electrodes, they are generally nonporous and have poor electrical conductivity and low extracellular electron transfer efficiency compared to noble metals. The carbon-based anodes are hybridized with carbon nanotubes (*45*–*48*), graphene (*28*, *49*, *50*), noble metal nanoparticles (*51*, *52*), and conductive polymers (*53*, *54*) to improve bacteria loading capacity and promote the direct electron transfer. Modification of the

[1]State Key Laboratory of Urban Water Resource and Environment (Harbin Institute of Technology), Harbin 150080, China. [2]School of Materials Science and Engineering, Harbin Institute of Technology, Harbin 150080, China. [3]CAS Key Laboratory of Nanosystem and Hierarchical Fabrication, National Center for Nanoscience and Technology, Beijing 100190, China. [4]Key Laboratory of Urban Pollutant Conversion, Institute of Urban Environment, Chinese Academy of Sciences, Xiamen 361021, China.
*These authors contributed equally to this work.
†Corresponding author. E-mail: shaoqinliu@hit.edu.cn (S.L.); zytang@nanoctr.cn (Z.T.)

anodes results in enhancement of the electrode surface area, reduction of the internal resistance, and thereby increase of the MFC efficiencies. Nevertheless, novel material and structure design about the anodes are highly desirable to further improve MFCs performance and life durability for practical application.

Here, we reported three-dimensional (3D) graphene aerogel (GA) decorated with platinum nanoparticles (Pt NPs) as an efficient free-standing anode for MFCs. The proposed GA-based anode has a continuous 3D macroporous structure that is favorable for microorganism immobilization and efficient electrolyte transport. Moreover, to further enhance extracellular charge transfer between the bacteria and the anode, GA scaffold is homogenously decorated with Pt NPs. The charge transfer capability of Pt NPs benefits the transfer and collection of the generated electrons to the anode (*51*, *52*). As a result, the MFCs constructed with the 3D GA/Pt–based anode generate an exceptional high current density of 4.88 A/m^2 and power density of 1460 mW/m^2, and the possible mechanism involved is also discussed. Impressively, as a demonstration of the real application, the MFCs constructed with the GA/Pt anode successfully run a timer for the first time, which opens the avenue toward the real application of the MFCs.

RESULTS AND DISCUSSION

To prepare the 3D GA/Pt–based anode, we synthesized self-supported 3D GA according to the previously reported hydrothermal treatment of graphene oxide (GO) sheets (*55*, *56*). Raman spectrum survey reveals that GO in the product is reduced, and its conjugated structures are partly restored (fig. S1). Subsequently, 3D GA was decorated with Pt NPs using a facile and surfactant-free microwave-assisted polyol process (see Materials and Methods). The obtained GA/Pt exhibits remarkable mechanical property including high strength and excellent toughness and can be arbitrarily tailored into any shapes, such as cubes, cylinders, or strips to fit different device configurations (Fig. 1A). The microscopic structure of GA/Pt is presented in Fig. 1B. It is noted that numerous flexible graphene sheets cross over each other to form characteristic 3D open porous architectures. Higher magnification (Fig. 1C) reveals that the pores with sizes ranging from several micrometer to tens of micrometer are interconnected, which are large enough to allow for internal colonization of *Shewanella oneidensis* MR-1 [the size of *S. oneidensis* MR-1 is about 0.5 μm × 2.5 μm (*36*)] as well as efficient electrolyte transport. Transmission electron microscopy (TEM) images (Fig. 1, D and E) further disclose that the Pt NPs with monodisperse sizes of 2.5 ± 0.3 nm are uniformly distributed on the surface of graphene sheets. The loading amount of Pt NPs has an important influence on electronic conductivity, roughness, and hydrophilic property of GA; hence, it would affect the inoculation of bacteria cells onto the surface of the electrode, sustainability of the bacteria cells in the the electrode environment, as well as electrode transfer rate and durability (*52*, *57*–*60*). So, the composition of the GA/Pt is analyzed by the energy dispersive spectroscopy (EDS) and the inductively coupled plasma–mass spectra (ICP-MS). EDS analysis confirms that the products are composed of C(93.20 atomic %), O (5.60 atomic %), and Pt (1.20 atomic %) (Fig. 1F). ICP-MS result shows that the loading of Pt is about 16.61 wt % in GA/Pt, which is very close to that obtained by the EDS measurement.

To examine the conductivity and diffusion of as-synthesized anode materials, we used electrochemical impedance spectroscopy (EIS) to

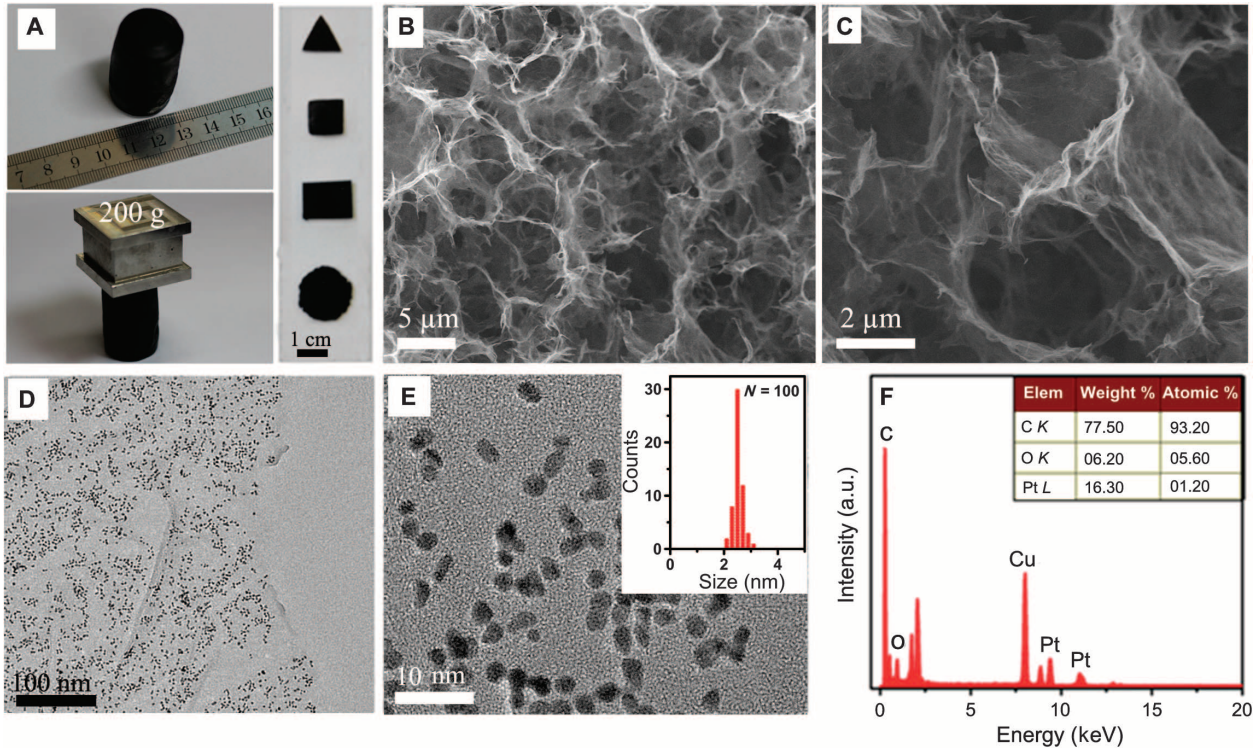

Fig. 1. The physical characterization of GA/Pt. (**A**) Digital photos of GA/Pt. (**B** and **C**) SEM and magnified SEM images of GA/Pt. (**D** and **E**) TEM and high-resolution TEM images of GA/Pt. (E) Inset: size distribution of Pt. (**F**) Energy-dispersive x-ray spectrum of GA/Pt, and the inset summarizes the content of C, O, and Pt elements. a.u., arbitrary units.

study the electrochemical behavior of GA and GA/Pt along with widely used carbon cloth anode. The results are plotted as Nyquist curves and further fitted with an equivalent circuit (Fig. 2 and the inset). Each EIS curve is composed of a well-defined semicircle followed by a straight line. The intercept of the semicircle with the real impedance axis presents the total ohmic resistance (R_{ohm}) of the electrochemical cell including the solution resistance (R_s) and the charge transfer resistance (R_{ct}) at the electrode/electrolyte interface (*61*). The R_{ohm} of GA/Pt anode is estimated to be ~68.7 ohms (Fig. 2), much lower than that of carbon cloth materials (~2790.6 ohms) and pure GA (~102.7 ohms). Moreover, the R_{ct} at the electrode/electrolyte interface, corresponding to the diameter of the semicircles, follows the order of carbon cloth (~2729.2 ohms) > GA (~42.9 ohms) > GA/Pt (~8.2 ohms). Because all three electrodes share the same setup and the same electrolyte, the decrease in the R_{ct} from ~42.9 ohms for GA to ~8.2 ohms for GA/Pt can only be attributed to the presence of Pt NPs. This result highlights the effectiveness of Pt NPs in enhancing charge transfer ability of GA. Except for R_{ohm} and R_{ct}, the ion diffusion resistance is also an important parameter to contribute to the total internal resistance, which causes the power or energy losses in MFCs (*62*, *63*). The ion diffusion coefficient (D) can be calculated from the plots in the low-frequency region (the straight line region in Fig. 2) based on Eqs. (1) and (2) (*64*, *65*)

$$Z' = R_s + R_{ct} + \sigma_w \omega^{-0.5} \quad (1)$$

$$D = R^2 T^2 / (2 S^2 F^4 \sigma_w^2 C^2) \quad (2)$$

where Z' is the real part of the impedance, ω is the angular frequency, and σ_w represents the slope of Z' against $\omega^{-0.5}$. R, F, T, S, and C are gas constant, Faraday constant, absolute temperature, surface area, and molar concentration of electrolyte ions, respectively. Thus, the D of GA/Pt, GA, and carbon cloth is estimated to be 1.45×10^{-7} cm^2/s, 4.62×10^{-8} cm^2/s, and 3.31×10^{-10} cm^2/s, respectively. Notably, one can see the two-order-of-magnitude improvement of D values of GA/Pt and GA over carbon cloth, which should be attributed to easy ion diffusion in 3D porous structure of GA/Pt and GA. Together, the EIS analysis reveals that GA/Pt composites with small charge transfer resistance and good ion diffusion coefficient would be ideal anode materials for high-performance MFCs.

To further evaluate the bacteria loading capacity and biocompatibility of the 3D GA/Pt composites, after incubation with *S. oneidensis* MR-1 for 3 days, we cut both GA/Pt and GA samples and we examined their interior. The scanning electron microscopy (SEM) images of GA/Pt (fig. S2 and Fig. 3A) clearly show that the entire surface of GA/Pt is covered with rod-shaped bacteria cells. The magnified SEM images of the cross section of GA/Pt (Fig. 3B and fig. S2, B and C) and GA (fig. S3) reveal that the interior surfaces of GA/Pt and GA are also fully covered with rod-shaped bacteria cells without clogging the macropores. These observations prove that the open macroporous structure of GA/Pt and GA has high bacteria loading capacity and allows for sufficient substrate transport to maintain internal colonization. As for the commercial carbon cloth, the bacteria biofilms are formed only on the surfaces or cracks (Fig. 3C), which are caused by a relatively smooth surface, small specific surface area, and low porosity of the carbon cloth. The good biocompatibility of the GA/Pt composites is further confirmed with the stained assay with calcein AM and PI to distinguish the live (green) and dead/apoptotic cells (red), respectively (see the detailed explanation in Materials and Methods). Figure 3D presents the CLSM image of bacteria immobilized on the interior surfaces of GA/Pt. It can be found that almost no death is observed in the bacteria cells, indicating the good biocompatibility of GA/Pt composites (Fig. 3D).

The outstanding charge transfer ability and good biocompatibility with macroporous 3D structure of GA/Pt satisfies the ideal MFC anode configuration. We then constructed the conventional H-shaped two-chamber MFCs by directly adopting the synthesized GA/Pt composites as freestanding anodes. The GA/Pt electrode inoculated with *S. oneidensis* MR-1 was positioned in the anodic chamber fed with M9 buffer solution containing 18 mM sodium lactate. The cathode was Pt sheet electrode (1 cm × 1 cm), and the cathodic chamber was fed with potassium hexacyanoferrate ($K_3[Fe(CN)_6]$, 50 mM) and potassium chloride (KCl, 50 mM) solutions. The uncolonized GA/Pt anode was initially inactive (Fig. 4A). After microbial inoculation with *S. oneidensis* MR-1 for 8 days, the open circuit voltage of MFCs increased to more than 0.3 V across a 1-kilohm resistor, indicating a successful startup (*45*). When the MFCs achieved stable power generation, its long-term stability was investigated. The anode chamber was operated in fed-batch mode, and

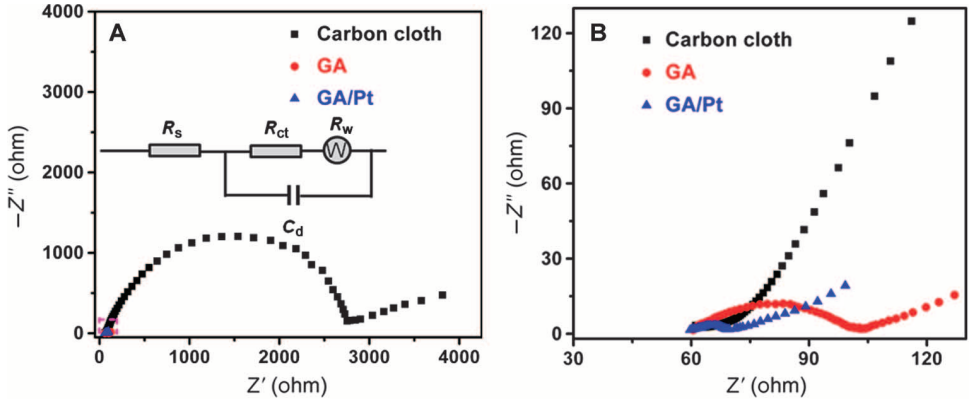

Fig. 2. Conductivity measurement of GA/Pt. (**A**) Nyquist plots of GA, GA/Pt, and carbon cloth. The ac impedance spectra are fitted with an equivalent circuit (inset), where R_s is the ohmic resistance of the electrolyte. C_d reflects the interfacial capacitance. R_{ct} and R_W are the charge transfer resistance of the anode material and the Warburg impedance of ion diffusion in the electrode, respectively. (**B**) Amplified Nyquist plots of the three samples. Compared with the GA and carbon cloth, Nyquist plot analysis indicates that the GA/Pt anode with small charge transfer resistance and good ion diffusion coefficient would be an ideal anode material for high-performance MFCs.

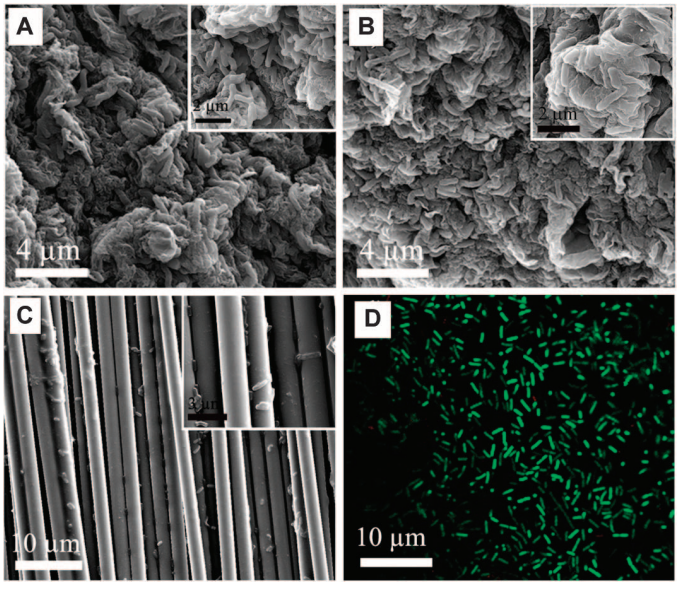

Fig. 3. The bacteria loading capacity and biocompatibility of GA/Pt. (**A**) SEM image of the surface of GA/Pt incubation with *S. oneidensis* MR-1 (inset: magnified SEM image). (**B**) SEM image of the cross section of GA/Pt incubation with *S. oneidensis* MR-1 (inset: magnified SEM image), revealing that the open macroporous structure of GA/Pt has high bacteria loading capacity. (**C**) SEM image of carbon cloth anode incubation with *S. oneidensis* MR-1 (inset: magnified SEM image). By comparing with the traditional carbon cloth under the same culture conditions, the advantage of GA/Pt for bacteria loading capacity is very obvious. (**D**) Confocal laser scanning microscope (CLSM) image of bacteria on GA/Pt after 3 days of colonization. The biocompatibility of GA/Pt composites is confirmed with the stained assay with calcein AM and propidium iodide (PI) to distinguish the live (green) and dead (red), respectively. CLSM image shows that bacteria can live very well on the GA/Pt.

the fresh medium was added when the current decreased to <0.5 μA. Figure 4B displays the typical power generation profile. The power density of the MFC with GA/Pt anode reaches 1193 mW/m^2 immediately after lactate injection and sharply decreases after running for about 100 hours because of depletion of sodium lactate. After refreshing the culture medium, the power density of the MFC quickly recovers to the initiated value of 1197 mW/m^2. Repeatable power generation cycles demonstrate the excellent stability of GA/Pt anode for electricity harvesting. The SEM image of the GA/Pt anode after 25 days of operation (three power generation cycles) indicates that the bacteria cells firmly adhere to the macroporous architecture of the GA/Pt and form a thick biofilm but do not clog the macroscale pores (Fig. 4C). Moreover, a great number of microbial nanowires were observed under SEM imaging. These nanowires tethered cells to the anode surface or to other cells, providing a probable direct path for extracellular electron transfer (*66*–*69*).

The long-term stability of the MFC with different substrate concentration has also been investigated. It is found that varied substrate concentration does not change the power density of MFCs; however, increasing the concentration of sodium lactate from 18 mM to 36 or 180 mM can result in longer running time (fig. S4). For example, the power density of the MFC with GA/Pt anode in 36 mM sodium lactate starts to decrease after running for about 200 hours, whereas the electrodes with abundant sodium lactate (180 mM) can be operated for more than 750 hours (ca. 31 days). The above results demonstrate that the decrease in the power density of the MFC with GA/Pt anode is ascribed to depletion of sodium lactate, which is the only electron donor source for the *S. oneidensis* MR-1 in the MFC system. That is, the content of electron donor source is the dominating factor responsible for the degradation of the MFC under the ideal condition (*70*). As demonstrated in fig. S4, the MFC with GA/Pt anode still keeps the initiated value of 1198 mW/m^2 after 43 days of operation, highlighting the excellent stability of GA/Pt anode for electricity harvesting. Such high durability of GA/Pt anode would greatly benefit the practical application.

The alive-dead stained assay further reveals that almost all microorganisms remain alive (Fig. 4D), strongly suggesting that the good biocompatibility of the 3D macroporous architecture is responsible for the excellent stability of GA/Pt anode for electricity harvesting. For comparison, we also investigated the electricity harvesting efficiency of GA- and carbon cloth–based MFCs under identical conditions (fig. S5). As shown in fig. S5, although both the GA and commercial carbon cloth anode could produce power, the current density of MFCs constructed with GA/Pt anodes (2372 mA/m^2) is 1.6 and 6.0 times higher than that of the GA anode (1481 mA/m^2) and the commercial carbon cloth anode (395 mA/m^2). The coulomb efficiency of GA/Pt, GA, and carbon cloth anode is estimated to be 69.3, 42.6, and 8.1%, respectively (see the detailed calculation process in the Supplementary Materials), so it is evident that the electricity conversion efficiency of GA/Pt anode is higher than that of GA and carbon cloth. The superior performance of GA/Pt should originate from good biocompatibility and high electron transfer efficiency between the bacteria and the GA/Pt anode (see the possible mechanism and detailed description in fig. S6).

The power density and polarization curves of three anodes (GA/Pt, GA, and carbon cloth) were determined by varying the external load resistance (0.01 to 99999 ohms). As demonstrated in Fig. 5A, the MFC equipped with GA/Pt anode delivers a remarkable maximum power density of 1460 mW/m^2, 5.3 times higher than that based on carbon cloth (273 mW/m^2) and 1.8 times higher than that based on GA (811 mW/m^2). Moreover, the maximum current density of the GA/Pt anode (4.88 A/m^2) is 5.5 times higher than that of the carbon cloth anode (0.88 A/m^2). These data strongly suggest that the GA/Pt anode enables the superior performance among all the reported MFCs inoculated with *S. oneidensis* MR-1 (table S1). Furthermore, the GA/Pt composites can be easily made in any size (as shown in Fig. 1A), which makes them ideal as anodes for small- or large-scale MFC applications. To exemplify the real application of the MFCs, two single biofuel cells have been assembled in series and successfully run a timer (Fig. 5B and movie S1). To the best of our knowledge, this is the first report to show that MFCs could drive the electrical devices.

Finally, we preliminarily examine the power generation capability of the MFC fed with wastewater. The effluent from the primary settling tanks in a municipal wastewater treatment facility (Gaobeidian Wastewater Treatment Plant, Beijing) is directly used as fuels without any pretreatment (fig. S7). Impressively, the maximum current and power density of the MFC fed with primary effluent can be up to 3.1 A/m^2 and 1064 mW/m^2, respectviely, verifying the potential in the practical wastewater treatment. Future work will be focused on rationalization of 3D GA/Pt architecture (such as their longevity in wastewater, reactor design, and reaction temperature) for large-scale MFC applications.

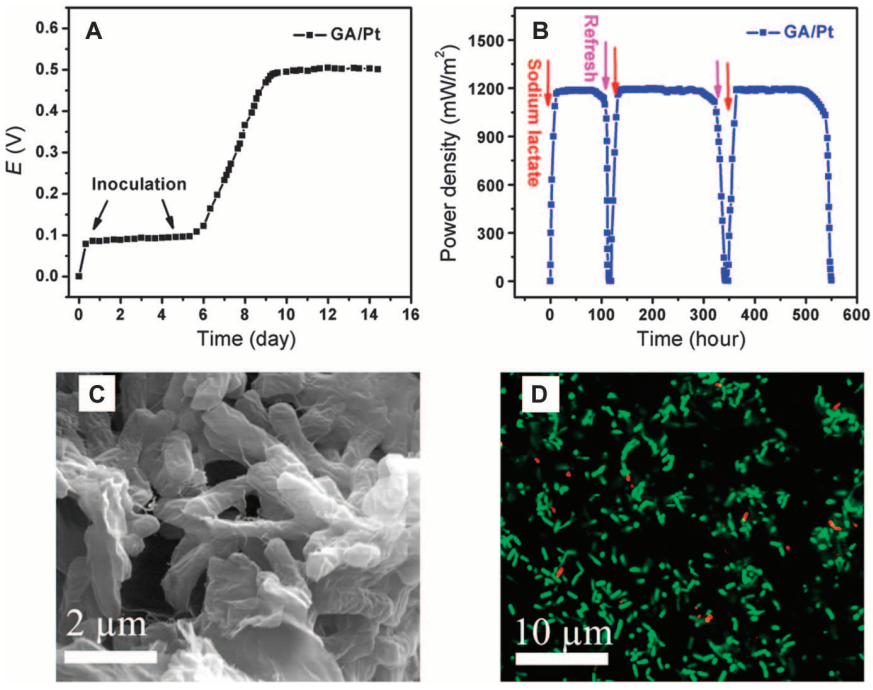

Fig. 4. The stability and repeatability of MFC constructed with GA/Pt. (**A**) Voltage generation of MFC across a 1-kilohm external resistor, and an operating voltage higher than 0.3 V indicates successful startup. (**B**) Repeatable power generation cycles with a 1-kilohm loading. Red and pink arrows point to sodium lactate feeding and refresh. (**C**) SEM image of bacteria on GA/Pt anode after 25 days of operation. The bacteria cells firmly adhere to the macroporous architecture of the GA/Pt and form a thick biofilm after 25 days of operation. (**D**) CLSM image of bacteria on GA/Pt anode after 25 days of colonization. After 25 days of operation, almost all of the bacteria are live (green) and few are dead because of the normal apoptotic cells.

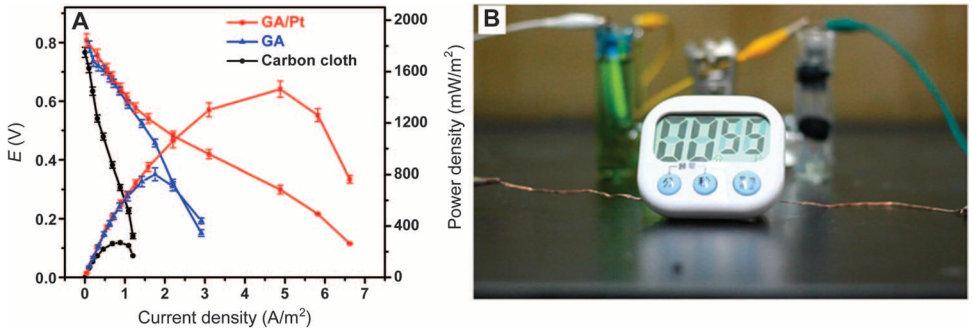

Fig. 5. The single-cell performance testing of MFCs and its application. (**A**) MFC single-cell performance constructed with different electrode materials working at room temperature. The current density (A/m^2) was obtained by using the measured current (three times) and the electrode area. (**B**) Digital photo of MFCs to drive a timer. The two single biofuel cells have been assembled in series and successfully run a timer, strongly exemplifying that the GA/Pt anode enables the superior performance and the actual application potential.

CONCLUSIONS

In summary, we propose the 3D porous GA decorated with Pt NPs as a novel and high-performance anode of MFCs. The MFCs equipped with the GA/Pt anode reach a current density of 4.88 A/m^2 and generate a maximum power density of 1460 mW/m^2 in sodium lactate medium, much higher than that obtained from the carbon cloth or pure GA under the same conditions. Detailed structural and electrochemical characterizations elucidate that the excellent performance of the GA/Pt anode is attributed to its high bacteria loading capacity, easy extracellular electron transfer between the cytochrome protein of the bacteria and the GA/Pt, as well as fast ion diffusion in 3D pores. Notably, we demonstrate that the MFCs constructed with the GA/Pt anode successfully run a timer. This is the first reported MFC in the literature to run an electrical device, which opens the avenue toward the real application of the MFCs.

MATERIALS AND METHODS

Materials

Graphite powder (natural briquetting grade of 99.999% purity) and $H_2PtCl_6 \cdot 6H_2O$ were purchased from Alfa Aesar. Ultrapure water (Millipore Milli-Q grade) with a resistivity of 18.2 megohms was used in all the experiments. GO was prepared from the graphite powder according to Hummers' method.

Synthesis of 3D architectures of GA

First, 60 ml of GO aqueous solution (2 mg/ml) was mixed with 100 μl of $NH_3 \cdot H_2O$ under mild ultrasonication. The mixture solution was then heated at 180°C for 12 hours to form GA. After the product was dialyzed with ultrapure water for at least 1 day, it was subjected to freeze-drying to generate 3D GA.

Synthesis 3D architectures of GA/Pt anode

3D GA (80 mg) was dispersed in 60 ml of ethylene glycol followed by addition of 1.5 ml of 80 mM H_2PtCl_6. After the mixture solution was stirred for 1 hour, its pH value was adjusted to 11 by adding 1 M NaOH solution. After the mixture was gently stirred for another 12 hours, it was placed in a microwave oven (CEM Voyager, 800 W) and heated by microwave irradiation for 60 s. Finally, the resulting GA/Pt anode was taken out, washed with deionized water, and dried in a vacuum oven at 60°C for 12 hours.

Physical characterization

TEM imaging was performed on an FEI Tecnai G2 F20 electron microscope operated at 200 kV. The surface morphology was observed with a Hitachi S4800 SEM. The ICP-MS were conducted with NEXION 300X. The GA/Pt after incubation with bacteria was fixed by immersion in 2.5% glutaraldehyde solution [5 ml of 50% glutaraldehyde, 45 ml of water, 45 ml of 0.2 mM phosphate-buffered saline (PBS) buffer] overnight at 4°C and chemically dehydrated using ethanol (30, 50, 70, 85, and 95% for one time, 100% for two times) with gradient concentration. The sample was dried in air and finally sputter-coated with 10-nm gold for SEM imaging. The EIS was recorded in PBS buffer (pH 7.02) using CHI 660D electrochemical working station (Chen Hua, Shanghai, China) with saturated calomel electrodes as a reference electrode. EIS was measured at the open circuit voltage in the frequency range of 10^5 to 0.05 Hz with a 10-mV peak-to-peak sinusoidal potential perturbation. The results were reported as Nyquist plots.

Bacteria culture

S. oneidensis MR-1 was purchased from the American Type Culture Collection (ATCC 700550) and stored at −80°C before use. *S. oneidensis* MR-1 was first grown in NB medium [Nutrient Broth, Bacto Tryptone (10 g/liter), beef extract (3 g/liter), NaCl (5 g/liter)] for 12 hours and then streaked onto NA [Nutrient Agar, Bacto Tryptone (10 g/liter), beef extract (3 g/liter), NaCl (5 g/liter), agar (15 g/liter)] plates. The resulting colonies were inoculated in 200 ml of fresh NB and incubated with shaking at 37°C until the OD600 (optical density at 600 nm) reached about 1.0.

MFC experiment

H-shaped two-chamber MFC, which was constructed by connecting two 50-ml L-shaped media tubes 2.5 cm in diameter and separated by Nafion membrane, was used in this work. The cathode was Pt sheet electrode (1 cm × 1 cm), and the cathodic chamber was fed with potassium hexacyanoferrate ($K_3[Fe(CN)_6]$, 50 mM) and potassium chloride (KCl, 50 mM) solutions. The anode was blank or preinoculated GA/Pt (1.5 cm × 1.5 cm), GA (1.5 cm × 1.5 cm), or carbon cloth (1.5 cm × 3.0 cm). In the case of the blank anode, the 5-ml bacteria solution, in which OD600 reached 1.0, was pelleted by centrifugation, washed with M9 buffer [10 mM succinic acid, 5.7 mM Na_2HPO_4, 3.3 mM KH_2PO_4, 18 mM NH_4Cl, 1 mM $MgSO_4$, and L-cysteine (0.02 g/liter)], and resuspended in 45 ml of M9 buffer supplemented with 18 mM lactate. The NB medium (5 ml) was then added to the above buffer solution and purged with pure nitrogen gas for 30 min to remove the dissolved oxygen. The anodic chamber was tightly sealed to maintain the anaerobic condition during the MFC operation. In the case of preinoculated anode, the sterile GA/Pt anode was first inoculated in 200 ml of fresh NB with the resulting colonies on the NA plates. When OD600 of bacteria reached about 1.0, the preinoculated GA/Pt was moved to the anode chamber of MFC for electricity harvesting. The electrolyte was 45 ml of M9 buffer containing 18 mM sodium lactate and 5 ml of NB solution. All the MFCs were operated on laboratory bench tops at ambient temperatures (~25°C). The anode and the cathode were connected through a variable external resistance of 0.01 to 99999 ohms, and the voltage across the resistor was monitored with digital multimeter (DT 9205A$^+$). At the steady state of MFC, the polarization curves were obtained by varying the external resistor. The measured potential was converted to an electric current using the following equation: $I = V$ (output voltage)$/R$ (external resistance). We calculated the current density (A/m^2) using the measured current and the electrode area. The power density (P) (W/m^2) was obtained by the following equation: $P = V \times I$.

CLSM measurement

The live-dead assay was used to evaluate the bacteria viability on the GA/Pt composite. The GA/Pt after incubation with bacteria for different times was crushed into small pieces, rinsed with PBS, and stained with calcein AM (Invitrogen) and PI (Invitrogen), respectively. The stained cells were examined using a Leica TCS SP5 II confocal/multiphoton laser scanning microscope (Germany). The live-dead assay solution was prepared by diluting calcein AM (1 mM solution in dimethyl sulfoxide) and PI (1.5 mM solution in deionized water) stock solutions in PBS at final concentrations of 2.0 and 4.0 μM. Calcein AM is a cell-permeant and nonfluorescent compound that was widely used for determining cell viability. In live cells, the nonfluorescent calcein AM was hydrolyzed by intracellular esterases into the strongly green fluorescent anion calcein. The fluorescent calcein was well retained in the cytoplasm in live cells. PI, a red fluorescence dye (excitation/emission maxima of ~535/617 nm when bound to DNA), was used to differentiate necrotic, apoptotic, and normal cells.

SUPPLEMENTARY MATERIALS

Supplementary material for this article is available at http://advances.sciencemag.org/cgi/content/full/1/10/e1500372/DC1

Fig. S1. Raman spectra of GO and GA.

Fig. S2. SEM images of GA/Pt incubated with *S. oneidensis* MR-1.

Fig. S3. SEM images of bacteria on GA with different magnifications.

Fig. S4. Long stability power generation profile of MFC by adding 18, 36, or 180 mM sodium lactate in fed-batch mode.

Fig. S5. Power generation profiles of MFCs constructed with carbon cloth (dark), GA (green), and GA/Pt anodes (red).

Fig. S6. Illustration of possible mechanism involving GA/Pt anode for enhancing the MFC performance.

Fig. S7. MFC single-cell performance fed with primary effluent.

Table S1. Summary of the performance of the previously reported MFCs inoculated with *S. oneidensis* MR-1.

Movie S1. The real application of the MFCs for running a timer.

References (*71*–*81*)

REFERENCES AND NOTES

1. P. L. McCarty, J. Bae, J. Kim, Domestic wastewater treatment as a net energy producer-can this be achieved? *Environ. Sci. Technol.* **45**, 7100–7106 (2001).
2. J. E. Castro, L. Heller, in *Water and Sanitation Services: Public Policy and Management* (Earthscan, London, 2009).

3. B. E. Logan, Exoelectrogenic bacteria that power microbial fuel cells. *Nat. Rev. Microbiol.* **7**, 375–381 (2009).
4. M. Rosenbaun, F. Zhao, U. Schröder, F. Scholz, Interfacing electrocatalysis and biocatalysis with tungsten carbide: A high-performance, noble-metal-free microbial fuel cell. *Angew. Chem. Int. Ed.* **45**, 6658–6661 (2006).
5. H. Hou, X. Chen, A. W. Thomas, C. Catania, N. D. Kirchhofer, L. E. Garner, A. Han, G. C. Bazan, Conjugated oligoelectrolytes increase power generation in *E. coli* microbial fuel cells. *Adv. Mater.* **25**, 1593–1597 (2013).
6. B. E. Logan, K. Rabaey, Conversion of wastes into bioelectricity and chemicals by using microbial electrochemical technologies. *Science* **337**, 686–690 (2012).
7. T. O. Oh, J. R. Kim, G. C. Premier, T. H. Lee, C. Kim, W. T. Sloan, Sustainable wastewater treatment: How might microbial fuel cells contribute. *Biotechnol. Adv.* **28**, 871–881 (2010).
8. B. E. Logan, in *Microbial Fuel Cells* (John Wiley & Sons Inc., Hoboken, NJ, 2008).
9. B. E. Logan, J. M. Regan, Microbial fuel cells—Challenges and applications. *Environ. Sci. Technol.* **40**, 5172–5180 (2006).
10. A. Aldrovandi, E. Marsili, L. Stante, P. Paganin, S. Tabacchioni, A. Giordano, Sustainable power production in a membrane-less and mediator-less synthetic wastewater microbial fuel cell. *Bioresour. Technol.* **100**, 3252–3260 (2009).
11. D. Simonsson, Electrochemistry for a cleaner environment. *Chem. Soc. Rev.* **26**, 181–189 (1997).
12. O. Lefebvre, A. Uzabiaga, I. S. Chang, B.-H. Kim, H. Y. Ng, Microbial fuel cells for energy self-sufficient domestic wastewater treatment—A review and discussion from energetic consideration. *Appl. Microbiol. Biotechnol.* **89**, 259–270 (2011).
13. H. Liu, R. Ramnarayanan, B. E. Logan, Production of electricity during wastewater treatment using a single chamber microbial fuel cell. *Environ. Sci. Technol.* **38**, 2281–2285 (2004).
14. S. Cheng, B. E. Logan, Sustainable and efficient biohydrogen production via electrohydrogenesis. *Proc. Natl. Acad. Sci. U.S.A.* **104**, 18871–18873 (2007).
15. K. B. Gregory, D. R. Lovley, Remediation and recovery of uranium from contaminated subsurface environments with electrodes. *Environ. Sci. Technol.* **39**, 8943–8947 (2005).
16. A. Ter Heijne, F. Liu, R. van der Weijden, J. Weijma, C. J. N. Buisman, H. V. M. Hamelers, Copper recovery combined with electricity production in a microbial fuel cell. *Environ. Sci. Technol.* **44**, 4376–4381 (2010).
17. L. M. Tender, C. E. Reimers, H. A. Stecher III, D. E. Holmes, D. R. Bond, D. A. Lowy, K. Pilobello, S. J. Fertig, D. R. Lovley, Harnessing microbially generated power on the seafloor. *Nat. Biotechnol.* **20**, 821–825 (2002).
18. M. Mehanna, P. D. Kiely, D. F. Call, B. E. Logan, Microbial electrodialysis cell for simultaneous water desalination and hydrogen gas production. *Environ. Sci. Technol.* **44**, 9578–9583 (2010).
19. X. Cao, X. Huang, P. Liang, K. Xiao, Y. Zhou, X. Zhang, B. E. Logan, A new method for water desalination using microbial desalination cells. *Environ. Sci. Technol.* **43**, 7148–7152 (2009).
20. H. Luo, P. E. Jenkins, Z. Ren, Concurrent desalination and hydrogen generation using microbial electrolysis and desalination cells. *Environ. Sci. Technol.* **45**, 340–344 (2011).
21. J. J. Konikoff, L. W. Reynolds, E. S. Harris, Electrical energy from biological systems. *Aerosp. Med.* **34**, 1129–1133 (1963).
22. S. Choi, H.-S. Lee, Y. Yang, P. Parameswaran, C. I. Torres, B. E. Rittmann, J. Chae, A μL-scale micromachined microbial fuel cell having high power density. *Lab Chip* **11**, 1110–1117 (2011).
23. Y. Zhang, G. Mo, X. Li, W. Zhang, J. Zhang, J. Ye, X. Huang, C. Yu, A graphene modified anode to improve the performance of microbial fuel cells. *J. Power Sources* **196**, 5402–5407 (2011).
24. X. D. Benetton, S. G. Navarro-Ávila, C. Carrera-Figueiras, Electrochemical evaluation of Ti/TiO_2-polyaniline anodes for microbial fuel cells using hypersaline microbial consortia for synthetic-wastewater treatment. *J. New Mater. Electrochem. Sys.* **13**, 1–6 (2010).
25. A. ter Heijne, H. V. M. Hamelers, M. Saakes, C. J. N. Buisman, Performance of non-porous graphite and titanium-based anodes in microbial fuel cells. *Electrochim. Acta* **53**, 5697–5703 (2008).
26. L. Hu, Y. Cui, Energy and environmental nanotechnology in conductive paper and textiles. *Energy Environ. Sci.* **5**, 6423–6435 (2012).
27. S. Zhao, H. Yin, L. Du, L. He, K. Zhao, L. Chang, G. Yin, H. Zhao, S. Liu, Z. Tang, Carbonized nanoscale metal-organic frameworks as high performance electrocatalysts for oxygen reduction reaction. *ACS Nano* **8**, 12660–12668 (2014).
28. X. Xie, G. Yu, N. Liu, Z. Bao, C. S. Criddle, Y. Cui, Graphene-sponges as high-performance low-cost anodes for microbial fuel cells. *Energy Environ. Sci.* **5**, 6862–6866 (2012).
29. Z. Y. Tang, Y. Wang, P. Podsiadlo, N. A. Kotov, Biomedical applications of layer-by-layer assembly: From biomimetics to tissue engineering. *Adv. Mater.* **18**, 3203–3224 (2006).
30. A. Okamoto, K. Saito, K. Inoue, K. H. Nealson, K. Hashimoto, R. Nakamura, Uptake of self-secreted flavins as bound cofactors for extracellular electron transfer in *Geobacter* species. *Energy Environ. Sci.* **7**, 1357–1361 (2014).
31. H. Liu, S. Matsuda, S. Kato, K. Hashimoto, S. Nakanishi, Redox-responsive switching in bacterial respiratory pathways involving extracellular electron transfer. *ChemSusChem* **3**, 1253–1256 (2010).
32. C. Ding, H. Liu, Y. Zhu, M. Wan, L. Jiang, Control of bacterial extracellular electron transfer by a solid-state mediator of polyaniline nanowire arrays. *Energy Environ. Sci.* **5**, 8517–8522 (2012).
33. J. R. Kim, S. Cheng, S.-E. Oh, B. E. Logan, Power generation using different cation, anion, and ultrafiltration membranes in microbial fuel cells. *Environ. Sci. Technol.* **41**, 1004–1009 (2007).
34. X. Zhang, S. Cheng, X. Wang, X. Huang, B. E. Logan, Separator characteristics for increasing performance of microbial fuel cells. *Environ. Sci. Technol.* **43**, 8456–8461 (2009).
35. F. Li, Y. Sharma, Y. Lei, B. Li, Q. Zhou, Microbial fuel cells: The effects of configurations, electrolyte solutions, and electrode materials on power generation. *Appl. Biochem. Biotechnol.* **160**, 168–181 (2010).
36. X. Jiang, J. Hu, A. M. Lieber, C. S. Jackan, J. C. Biffinger, L. A. Fitzgerald, B. R. Ringeisen, C. M. Lieber, Nanoparticle facilitated extracellular electron transfer in microbial fuel cells. *Nano Lett.* **14**, 6737–6742 (2014).
37. S. K. Chaudhuri, D. R. Lovley, Electricity generation by direct oxidation of glucose in mediator-less microbial fuel cells. *Nat. Biotechnol.* **21**, 1229–1232 (2003).
38. S. Cheng, H. Liu, B. E. Logan, Increased power generation in a continuous flow MFC with advective flow through the porous anode and reduced electrode spacing. *Environ. Sci. Technol.* **40**, 2426–2432 (2006).
39. D. Jiang, B. Li, Novel electrode materials to enhance the bacterial adhesion and increase the power generation in microbial fuel cells (MFCs). *Water Sci. Technol.* **59**, 557–563 (2009).
40. F. Zhao, N. Rahunen, J. R. Varcoe, A. Chandra, C. Avignone-rossa, A. E. Thumser, R. C. T. Slade, Activated carbon cloth as anode for sulfate removal in a microbial fuel cell. *Environ. Sci. Technol.* **42**, 4971–4976 (2008).
41. Y.-C. Yong, X.-C. Dong, M. B. Chan-Park, H. Song, P. Chen, Macroporous and monolithic anode based on polyaniline hybridized three-dimensional graphene for high-performance microbial fuel cells. *ACS Nano* **6**, 2394–2400 (2012).
42. H. R. Luckarift, S. R. Sizemore, K. E. Farrington, J. Roy, C. Lau, P. B. Atanassov, G. R. Johnson, Facile fabrication of scalable, hierarchically structured polymer/carbon architectures for bioelectrodes. *ACS Appl. Mater. Interfaces* **4**, 2082–2087 (2012).
43. U. Schröder, J. Nieβen, F. Scholz, A generation of microbial fuel cells with current outputs boosted by more than one order of magnitude. *Angew. Chem. Int. Ed.* **42**, 2880–2883 (2003).
44. B. Lai, X. Tang, H. Li, Z. Du, X. W. Liu, Q. Zhang, Power production enhancement with a polyaniline modified anode in microbial fuel cells. *Biosens. Bioelectron.* **28**, 373–377 (2011).
45. X. Xie, L. Hu, M. Pasta, G. F. Wells, D. Kong, C. S. Criddle, Y. Cui, Three-dimensional carbon nanotube-textile anode for high-performance microbial fuel cells. *Nano Lett.* **11**, 291–296 (2011).
46. S. Inoue, E. A. Parrab, A. Higa, Y. Q. Jiang, P. Wang, C. R. Buied, J. D. Coatese, L. Lin, Structural optimization of contact electrodes in microbial fuel cells for current density enhancements. *Sens. Actuators A Phys.* **177**, 30–36 (2012).
47. X. Xie, M. Pasta, L. Hu, Y. Yang, J. McDonough, J. Cha, C. S. Criddle, Y. Cui Nano-structured textiles as high-performance aqueous cathodes for microbial fuel cells. *Energy Environ. Sci.* **4**, 1293–1297 (2011).
48. J. E. Mink, J. P. Rojas, B. E. Logan, M. M. Hussain, Vertically grown multiwalled carbon nanotube anode and nickel silicide integrated high performance microsized (1.25 μL) microbial fuel cell. *Nano Lett.* **12**, 791–795 (2012).
49. J. Liu, Y. Qiao, C. X. Guo, S. Lim, H. Song, C. M. Li, Graphene/carbon cloth anode for high-performance mediatorless microbial fuel cells. *Bioresour. Technol.* **114**, 275–280 (2012).
50. L. Xiao, J. Damien, J. Luo, H. D. Dong, J. Huang, Z. He, Crumpled graphene particles for microbial fuel cell electrodes. *J. Power Sources* **208**, 187–192 (2012).
51. H. I. Park, U. Mushtaq, D. Perello, I. Lee, S. K. Cho, A. Star, M. Yun, Effective and low-cost platinum electrodes for microbial fuel cells deposited by electron beam evaporation. *Energy Fuels* **21**, 2984–2990 (2007).
52. Y. Fan, S. Xu, R. Schaller, J. Jiao, F. Chaplen, H. Liu, Nanoparticle decorated anodes for enhanced current generation in microbial electrochemical cells. *Biosens. Bioelectron.* **26**, 1908–1912 (2011).
53. Y. Qiao, S.-J. Bao, C. M. Li, X.-Q. Cui, Z.-S. Lu, J. Guo, Nanostructured polyaniline/titanium dioxide composite anode for microbial fuel cells. *ACS Nano* **2**, 113–119 (2008).
54. Y. Qiao, C. M. Li, S.-J. Bao, Q.-L. Bao, Carbon nanotube/polyaniline composite as anode material for microbial fuel cells. *J. Power Sources* **170**, 79–84 (2007).
55. Y. Xu, K. Sheng, C. Li, G. Shi, Self-assembled graphene hydrogel *via* a one-step hydrothermal process. *ACS Nano* **4**, 4324–4330 (2010).
56. H. Yin, S. Zhao, J. Wang, H. Tang, L. Chang, L. He, H. Zhao, Y. Gao, Z. Tang, Three-dimensional graphene/metal oxide nanoparticle hybrids for high-performance capacitive deionization of saline water. *Adv. Mater.* **25**, 6270–6276 (2013).
57. M. Grivet, J. J. Morrier, G. Benay, O. Barsotti, Effect of hydrophobicity on in vitro streptococcal adhesion to dental alloys. *J. Mater. Sci. Mater. Med.* **11**, 637–642 (2000).
58. C.-m. Ding, M.-l. Lv, Y. Zhu, L. Jiang, H. Liu, Wettability-regulated extracellular electron transfer from the living organism of *Shewanella loihica* PV-4. *Angew. Chem. Int. Ed.* **127**, 1466–1471 (2015).

59. G. G. Kumar, V. G. S. Sarathi, K. S. Nahm, Recent advances and challenges in the anode architecture and their modifications for the applications of microbial fuel cells. *Biosens. Bioelectron.* **43**, 461–475 (2013).
60. M. Sun, F. Zhang, Z.-H. Tong, G.-P. Sheng, Y.-Z. Chen, Y. Zhao, Y.-P. Chen, S.-Y. Zhou, G. Liu, Y.-C. Tian, H.-Q. Yu, A gold-sputtered carbon paper as an anode for improved electricity generation from a microbial fuel cell inoculated with *Shewanella oneidensis* MR-1. *Biosens. Bioelectron.* **26**, 338–343 (2010).
61. X. Dominguez-Benetton, S. Sevda, K. Vanbroekhoven, D. Pant, The accurate use of impedance analysis for the study of microbial electrochemical systems. *Chem. Soc. Rev.* **41**, 7228–7246 (2012).
62. Z. He, F. Mansfeld, Exploring the use of electrochemical impedance spectroscopy (EIS) in microbial fuel cell studies. *Energy Environ. Sci.* **2**, 215–219 (2009).
63. Y. Fan, H. Hu, H. Liu, Sustainable power generation in microbial fuel cells using bicarbonate buffer and proton transfer mechanisms. *Environ. Sci. Technol.* **41**, 8154–8158 (2007).
64. X. Xiao, P. Liu, J. S. Wang, M. W. Verbrugge, M. P. Balogh, Vertically aligned graphene electrode for lithium ion battery with high rate capability. *Electrochem. Commun.* **13**, 209–212 (2011).
65. C. Lin, X. Fan, Y. Xin, F. Cheng, M. O. Lai, H. Zhou, L. Lu, $Li_4Ti_5O_{12}$-based anode materials with low working potentials, high rate capabilities and high cyclability for high-power lithium-ion batteries: A synergistic effect of doping, incorporating a conductive phase and reducing the particle size. *J. Mater. Chem. A* **2**, 9982–9993 (2014).
66. G. Reguera, K. D. McCarthy, T. Mehta, J. S. Nicoll, M. T. Tuominen, D. R. Lovley, Extracellular electron transfer via microbial nanowires. *Nature* **435**, 1098–1101 (2005).
67. N. S. Malvankar, M. Vargas, K. P. Nevin, A. E. Franks, C. Leang, B.-C. Kim, K. Inoue, T. Mester, S. F. Covalla, J. P. Johnson, V. M. Rotello, M. T. Tuominen, D. R. Lovley, Tunable metallic-like conductivity in microbial nanowire networks. *Nat. Nanotechnol.* **6**, 573–579 (2011).
68. M. Y. El-Naggar, G. Wanger, K. M. Leung, T. D. Yuzvinsky, G. Southam, J. Yang, W. M. Lau, K. H. Nealson, Y. A. Gorby, Electrical transport along bacterial nanowires from *Shewanella oneidensis* MR-1. *Proc. Natl. Acad. Sci. U.S.A.* **107**, 18127–18131 (2010).
69. Y. A. Gorby, S. Yanina, J. S. McLean, K. M. Rosso, D. Moyles, A. Dohnalkova, T. J. Beveridge, I. S. Chang, B. H. Kim, K. S. Kim, D. E. Culley, S. B. Reed, M. F. Romine, D. A. Saffarini, E. A. Hill, L. Shi, D. A. Elias, D. W. Kennedy, G. Pinchuk, K. Watanabe, S. Ishii, B. Logan, K. H. Nealson, J. K. Fredrickson, Electrically conductive bacterial nanowires produced by *Shewanella oneidensis* strain MR-1 and other microorganisms. *Proc. Natl. Acad. Sci. U.S.A.* **103**, 11358–11363 (2006).
70. H. Li, J. Ni, Treatment of wastewater from *Dioscorea zingiberensis* tubers used for producing steroid hormones in a microbial fuel cell. *Bioresour. Technol.* **102**, 2731–2735 (2011).
71. S. Xu, H. Liu, Y. Fan, R. Schaller, J. Jun, F. Chaplen, Enhanced performance and mechanism study of microbial electrolysis cells using Fe nanoparticle-decorated anodes. *Appl. Microbiol. Biotechnol.* **93**, 871–880 (2011).
72. V. J. Watson, B. E. Logan, Power production in MFCs inoculated with *Shewanella oneidensis* MR-1 or mixed cultures. *Biotechnol. Bioeng.* **105**, 489–498 (2010).
73. A. Kouzuma, X.-Y. Meng, N. Kimura, K. Hashimoto, K. Watanabe, Disruption of the putative cell surface polysaccharide biosynthesis gene SO3177 in *Shewanella oneidensis* MR-1 enhances adhesion to electrodes and current generation in microbial fuel cells. *Appl. Environ. Microbiol.* **76**, 4151–4157 (2010).
74. J. E. Mink, M. M. Hussain, Sustainable design of high-performance microsized microbial fuel cell with carbon nanotube anode and air cathode. *ACS Nano* **7**, 6921–6927 (2013).
75. M. A. Rosenbaum, H. Y. Bar, Q. K. Beg, D. Segre, J. Booth, M. A. Cotta, L. T. Angenent, *Shewanella oneidensis* in a lactate-fed pure-culture and a glucose-fed co-culture with *Lactococcus lactis* with an electrode as electron acceptor. *Bioresour. Technol.* **102**, 2623–2628 (2011).
76. O. Bretschger, A. C. M. Cheung, F. Mansfeld, K. H. Nealson, Comparative microbial fuel cell evaluations of *Shewanella* spp. *Electroanalysis* **22**, 883–894 (2010).
77. C. Zhao, P. Gai, C. Liu, X. Wang, H. Xu, J. Zhang, J.-J. Zhu, Polyaniline networks grown on graphene nanoribbons-coated carbon paper with a synergistic effect for high-performance microbial fuel cells. *J. Mater. Chem. A* **1**, 12587–12594 (2013).
78. C. Zhao, Y. Wang, F. Shi, J. Zhang, J.-J. Zhu, High biocurrent generation in *Shewanella*-inoculated microbial fuel cells using ionic liquid functionalized graphene nanosheets as an anode. *Chem. Commun.* **49**, 6668–6670 (2013).
79. W.-W. Li, G.-P. Sheng, X.-W. Liu, P.-J. Cai, M. Sun, X. Xiao, Y.-K. Wang, Z.-H. Tong, F. Dong, H.-Q. Yu, Impact of a static magnetic field on the electricity production of *Shewanella*-inoculated microbial fuel cells. *Biosens. Bioelectron.* **26**, 3987–3992 (2011).
80. Y.-X. Huang, X.-W. Liu, J.-F. Xie, G.-P. Sheng, G.-Y. Wang, Y.-Y. Zhang, A.-W. Xu, H.-Q. Yu, Graphene oxide nanoribbons greatly enhance extracellular electron transfer in bioelectrochemical systems. *Chem. Commun.* **47**, 5795–5797 (2011).
81. Y.-Y. Yu, H.-I. Chen, Y.-C. Yong, D.-H. Kim, H. Song, Conductive artificial biofilm dramatically enhances bioelectricity production in *Shewanella*-inoculated microbial fuel cells. *Chem. Commun.* **47**, 12825–12827 (2011).

Acknowledgments: We thank the Center for the use of FEI Tecnai G2 F20 electron microscope and Hitachi S4800 SEM. **Funding:** We thank the Center for the use of FEI Tecnai G2 F20 electron microscope and Hitachi S4800 SEM. This work was financially supported by the National Research Fund for Fundamental Key Project (grant 2014CB931801), National Natural Science Foundation of China (grants 51372054, 21161120325, 21025310, and 51402069), and Outstanding Young Funding of Heilongjiang Province and State Key Laboratory of Urban Water Resource and Environment (Harbin Institute of Technology) (grant 2015TS03). **Author contributions:** S.L. and Z.T. proposed the research direction and guided the project. S.Z. and Y.L. designed and performed the experiments. Y.L. separated and purified *S. oneidensis* MR-1. S.Z., Y.L., and H.Y. analyzed and discussed the experimental results. S.Z., Y.L., S.L., and Z.T. wrote the manuscript. H.Y., Z.L., E.L., S.L., and F.Z. joined the discussion of data and gave some useful suggestions. **Competing interests:** The authors declare that they have no competing interests. **Data and materials availability:** All data needed to evaluate the conclusions in the paper are present in the paper and/or the Supplementary Materials. Additional data related to this paper may be requested from the authors.

Submitted 23 March 2015
Accepted 1 September 2015
Published 13 November 2015
10.1126/sciadv.1500372

Citation: S. Zhao, Y. Li, H. Yin, Z. Liu, E. Luan, F. Zhao, Z. Tang, S. Liu, Three-dimensional graphene/Pt nanoparticle composites as freestanding anode for enhancing performance of microbial fuel cells. *Sci. Adv.* **1**, e1500372 (2015).